buildings

MDPI

Article

CFD Study of Pressure Distribution on Recessed Faces of a Diamond C-Shaped Building

Arun Kumar [1], Rahul Kumar Meena [2], Ritu Raj [1], Mohammad Iqbal Khan [3,*] and Jamal M. Khatib [4]

[1] Department of Civil Engineering, Delhi Technological University, Delhi 110042, India; arunkumar.dtu@gmail.com (A.K.); rituraj@dtu.ac.in (R.R.)
[2] Department of Civil Engineering, Punjab Engineering College, Chandigarh 160012, India; rahul.08dtu@gmail.com
[3] Department of Civil Engineering, College of Engineering, King Saud University, P.O. Box 800, Riyadh 11421, Saudi Arabia
[4] Faculty of Science and Engineering, University of Wolverhampton, Wolverhampton WV1 1LY, UK; j.m.khatib@wlv.ac.uk
* Correspondence: miqbal@ksu.edu.sa

Abstract: A building situated in the flow path of the wind is subjected to differential velocity and pressure distribution around the envelope. Wind effects are influenced by and vary for each individual shape of a tall building. Tall building structures are considered as cantilever structures with fixed ends at the ground. Wind velocity acting along the height of the building makes the velocity and pressure distribution more complex; as the height of the building structure increases, wind velocity increases. This study discusses the effect of the wind on an irregular cross-section shape. The present study was conducted numerically with a building model placed in a virtual wind tunnel using the ANSYS (CFX 2020 Academic Version) software tool. Wind effects are investigated on a building model situated in a terrain category-II defined in IS: 875 (Part 3): 2015; wind scale model of 1:100 and turbulence intensity are at 5% and power law index α is considered to be 0.143. The validation and verification of the study were made by comparing pressure coefficients on different faces of a rectangular model of similar floor area and height as that taken for a C-plan dia-mond-shaped model under similar boundary conditions, wind environment, and solver setting of numerical setups. The values of surface pressures generated on the recessed faces of the model and wind flow patterns within the recessed cavity were studied at wind incident angles 0°, 30°, 60°, 105°, 135°, and 180°. The critical suction on all the recessed faces was observed to be at a 105° angle of wind attack.

Keywords: diamond C-shape tall building; wind loads; ANSYS (CFX); pressure coefficients

check for updates

Citation: Kumar, A.; Meena, R.K.; Raj, R.; Khan, M.I.; Khatib, J.M. CFD Study of Pressure Distribution on Recessed Faces of a Diamond C-Shaped Building. *Buildings* **2023**, *13*, 2800. https://doi.org/10.3390/buildings13112800

Academic Editors: Farid Abed and Abedulgader Baktheer

Received: 6 October 2023
Revised: 24 October 2023
Accepted: 3 November 2023
Published: 8 November 2023

Copyright: © 2023 by the authors. Licensee MDPI, Basel, Switzerland. This article is an open access article distributed under the terms and conditions of the Creative Commons Attribution (CC BY) license (https://creativecommons.org/licenses/by/4.0/).

1. Introduction

To fulfil the requirement of housing for all, high-rise building construction has become a necessity, especially in urban and metropolitan cities. It is essential to evaluate the wind impact on such high-rise buildings for the safety of the structure and the comfort of the users. In its most basic form, wind flow consists of a succession of gusts that vary greatly in amplitude and direction. Strong wind may cause discomfort to the users and damage to the structure. Extreme winds such as hurricanes, cyclones, and tornadoes can cause extensive damage to buildings due to the heavy load produced by such winds. The shape and size of the building play an important role in modifying the wind-produced load on the building. As the height of the building increases, the wind load increases, and it becomes the governing design factor for high-rise structure [1]. As such, it is important to study the wind environment on all types of high-rise buildings.

When the wind is motionless, normal air pressure acts everywhere around the building surfaces, balancing the load on the building in totality. As the wind gains momentum, pressure differentials manifest across the building's surfaces. In accordance with Bernoulli's

equation, the point of stagnation on the windward facade, where wind velocity diminishes to zero, corresponds to the location of peak pressure generation. This pressure is equal to $\frac{1}{2}\rho u^2$, where ρ and u are air density and wind speed respectively. This is known as velocity/impact pressure [2]. Using Bernoulli's equation, pressure differences at a point can be represented as:

$$C_{Pe} = \frac{\Delta P}{\rho u^2/2} \quad (1)$$

where, C_{Pe} is a dimensionless entity called pressure coefficient and ΔP is the pressure difference between the actual pressure at the point, P, and the normal atmospheric pressure P_o acting at that point. In the separated flow and wake regions where shear layers and vorticity do exist [3]. A good prediction of the pressure coefficient can be made by Equation (1). In the atmospheric boundary layer (ABL) flow, where an exponential rise in velocity field along the height occurs due to frictional resistance from the surface of the earth, pressure gradient, Coriolis effect, and earth's rotation, defining the velocity field is not an easy task. ABL is the distance from the mean surface of the earth up to which the exponential gradient velocity field exists. It is the reference height which is known as gradient height and at this height, wind speed is termed as the gradient wind. So, u is set at a reference height. The greatest velocity at the rooftop of the model was used to calculate all C_{Pe} values in the current study of the wind effects. Points corresponding to the highest C_{Pe}, where impact pressure is greatest, can be found in this manner. A larger pressure drop caused by gustiness of wind at any point causes the average pressure distribution over the windward surface to be greater than the impact pressure. The resulting coefficient is mostly unaffected by wind speed and model scale [2]. It is, however, influenced by the form of the building, wind flow direction, terrain roughness, and proximity to other structures [4]. For structural design purposes, we can find C_{Pe} values for regular plan-shaped buildings in different international codes/standards, but the data are available only for orthogonal directions of wind flow. The value of pressure coefficients given in the codes for structural design needs slight upgrading and the data for the regular shape structure are only provided. For various unconventional architectural shapes, nowadays being used by architects, the values of C_{Pe} are either presumed from the codes, which are relatively inaccurate as they are approximated from the shapes given in codes, or from wind tunnel experiments, which are costly and time-consuming. With the invention of complex computational facilities available nowadays, it is possible to know C_{Pe} values on buildings of different architectural shapes.

Various studies have been presented by different researchers, and some major findings are the pattern of wind velocity distribution and fluid pressure affect on tall buildings [5]. They demonstrated the isobars of the mean wind pressure on the windward face to be positive and suction pressures on the side faces, lee face, and rooftop of a tall square structure. The numerical study was presented using CFD modeling to examine how the flow patterns on L and U shape models changed across a wide range of wind incidence angles [6]. The surface pressure distributions were studied in a wind tunnel test. Wind flow in the recessed cavity of an H-shaped tall building using CFD was studied [7]. The wind-induced response and equivalent wind load on super tall buildings were investigated using experimental methods on building models [8]. The flow between the cavity and outside of the cavity for different aspect ratios were studied. The flow within the cavity was found to be neither simply a cross-flow nor a stagnation flow. It is reported the flow pattern was complex within the cavity and dependent upon the height and formation of two circulation vortices inside the cavity. L-shape and T-shape models of similar cross-sectional area and height but different limb lengths were investigated [9]. It was observed the cross-sectional shapes and limb lengths were crucial for pressure distribution on different faces. However, the magnitude of peak pressure and peak suction on the faces largely depended on wind direction. Mean interference of close proximity rectangular buildings placed near different shape buildings were studied by [10] in the wind tunnel for boundary layer wind flow over extended wind angles, and a comparison was made with the response

of similar buildings in isolation. Interference effects were reported to be influenced by the position and arrangements of models and wind incidence angles. Wind tunnel studies were used to illustrate the aerodynamic properties of several irregular plan shaped tall buildings [11]. A review of wind effects showed instruments were not accurate enough to identify wind load parameters in the nonlinear region [12]. A CFD study on ANSYS (CFX) was carried out at different wind angles on a rectangular model for interference effect due to another upstream rectangular model similar in plan area [13]. The wind effects on tall buildings were observed. The positive wind effects were on the windward side while negative pressure was on the leeward side [14]. It was observed that if the variation in the aspect ratio of interfering and principal building models was varied gradually from 1:5 to 5:5, the wind distribution on the windward side is more or less of the same nature while the leeward side and side faces of the tall building model represent slightly more variations. The validity of the research study was determined by comparing the pressure coefficients on the different surfaces of the building in isolation with different wind standards. It was revealed that the wind load on the principal building largely depends upon the aspect ratios of the principal and interfering buildings and wind incident angles. Wind pressure variations on the octagonal plan shape building model in isolated and interfering conditions were studied by using ANSYS (CFX) [15]. The wind pressure was determined by varying the geometry or exposure condition [16]. The wind effects were studies on a super tall building using an experimental method; it was found the twisted wind flow will vary the vortex shedding mainly on the wind ward and side faces [17]. A comparison of pressure on the faces and roofs of a square-tall building with different setback was studied by [18] using ANSYS (CFX). The setback roof was found to be subjected to higher pressure than the top of the roof. Wind effects were investigated using ANSYS (CFX) solver to examine the distribution of wind pressure on an E-plan-shape model [19]. According to the research study, the values of the coefficient of pressure on various faces for different element meshing sizes differ from wind tunnel measurements with some slight variation. Interference effects on an H-shape building model with similar building models placed at various positions were investigated [20]. At full blockage, suction produced on the main building was found to be higher than other blockage conditions. Modification of wind flow around two plus-shape tall building models was studied in a wind tunnel. The increase or decrease in wind load on the building façade was dependent on the relative positioning of the building models. In full blockage condition, more suction was reported to occur on the gap faces and severe interference effect was reported at half and no blockage condition. Mostly, research presented is either on the regular or some slight modification in the geometry while the present study is investigating the wind effects on a C-shape building model.

Mostly, studies are not available for the irregular type C-plan shape building model To investigate the structural behavior of super tall buildings under strong wind effects, it was observed that the turbulent intensity and gust factor decreased as the mean wind speed increased [21]. Experimental studies on C-shape building models of similar plan areas but different heights were investigated, and the findings from the current study were discussed [22]. It has been reported that geometry, aspect ratio, and wind flow pattern have a significant influence on pressure variations on faces. The goal of the current study was to determine how wind loads would affect a structure with a diamond C-plan shape building having a 300 sqm plan area and 50 m height (Figure 1a). The present study is performed using the numerical simulation on a building model using ANSYS (CFX) software by utilizing the standard k-ε turbulent model. C_{Pe} values obtained on the faces were evaluated for 0° to 180° at 15° wind attack angles. However, a brief description of the wind flow pattern and typical (critical) values of the coefficient of wind pressure on the recessed faces for 0°, 30°, 60°, 105°, 135°, and 180° wind attack angles are presented in this research study.

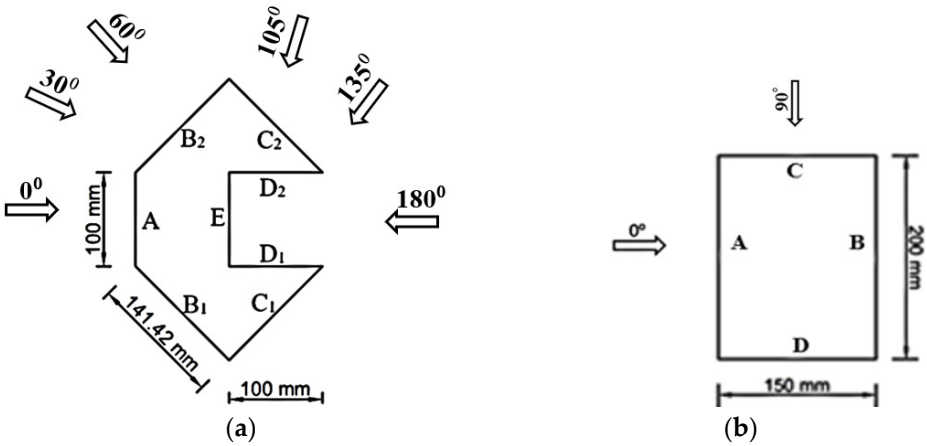

Figure 1. (**a**): Diamond C-shape Model, (**b**): Rectangular Model.

2. Verification and Validation

For validation and verification, a rectangular model (Figure 1b) of similar floor area and height was simulated under the same wind environment, boundary conditions, and solver setting. The power law was used to apply a homogeneous steady-state wind with 5% turbulence in the ABL of the terrain roughness mentioned in the abstract, with a roughness coefficient, $\alpha = 0.143$. Free wind velocity and turbulence intensity profiles along the height of the building model were plotted and compared with experimental data from [20] and are shown in Figures 2 and 3, respectively. A comparison of the C_{Pe} results on faces of the rectangular model for the two orthogonal directions of wind were compared with those in relevant codes of different countries and for a 90° wind angle from experimental data [23]. The results are presented in Table 1, and the data of mean pressure coefficient is compared with different international standards and experimental studies.

Table 1. Comparison of Area Average C_{Pe} on Faces of Rectangular Model.

As per	Wind Angle	C_{Pe} Face A	C_{Pe} Face B	C_{Pe} Face C	C_{Pe} Face D
ANSYX (CFX)	0°	+0.70	−0.28	−0.60	−0.60
	90°	−0.60	−0.60	+0.68	−0.27
IS: 875 (Part 3): 2015 [24]	0°	+0.8	−0.25	−0.8	−0.8
	90°	−0.8	−0.8	0.8	−0.25
ASCE/SEI 7−22 [25]	0°	+0.8	−0.5	−0.7	−0.7
	90°	−0.7	−0.7	0.8	−0.5
AS/NZS-1170.2 (2002) [26]	0°	+0.8	−0.5	−0.65	−0.65
	90°	−0.65	−0.65	0.8	−0.5
EN: 1991-1-4 [27]	0°	0.8	−0.55	−0.8	−0.8
	90°	−0.8	−08	0.8	−0.55
BS: 6399-2 [28]	0°	0.76	−0.5	−0.8	−0.8
Amin and Ahuja 2013 [23]	90°	−0.8	−0.8	0.76	−0.5
	90°	−0.66	−0.66	0.74	−0.41

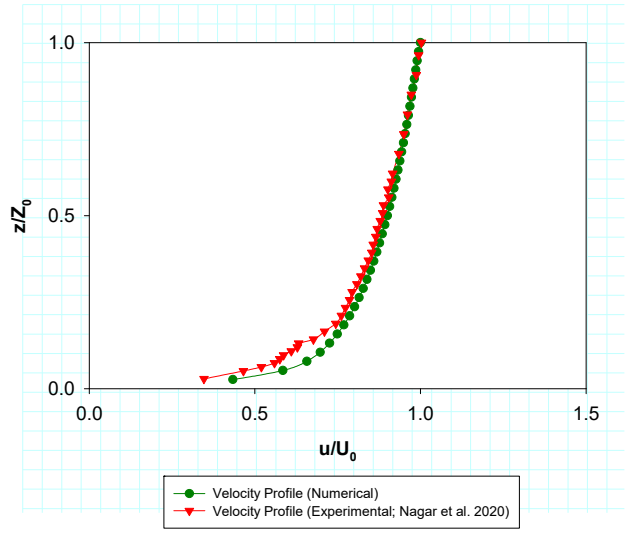

Figure 2. Mean Wind Velocity Profile [20].

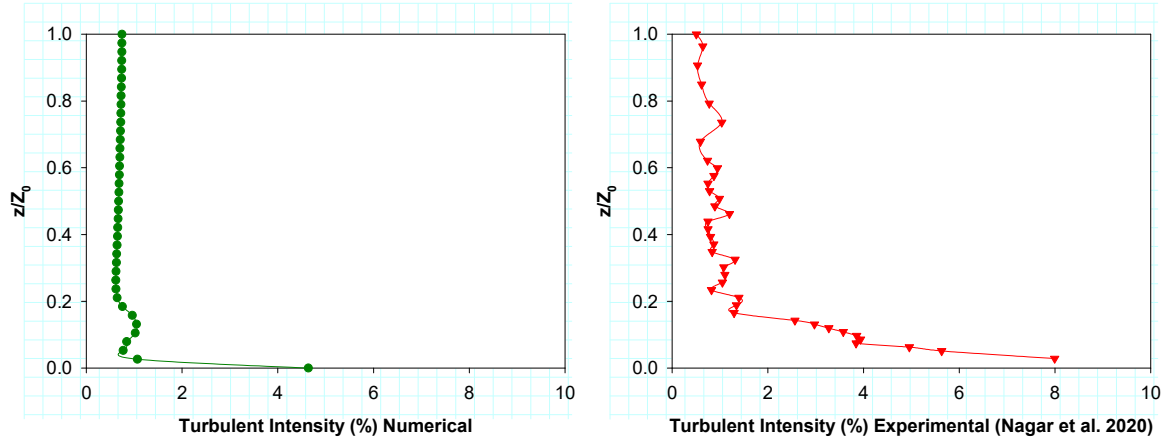

Figure 3. Mean Wind Turbulent Intensity Profile [20].

3. Numerical Analysis

Various mathematical models based on Navier-Stokes equations have been developed by researchers to study the flow simulation of fluids. These models have been presented in the form of differential equations which contain several unknowns and unmeasurable quantities that can be neglected. These differential equations are solved at finite grid locations during simulation. For bluff body wind simulation, the standard k—epsilon ($k-\varepsilon$) turbulence model is mostly used. It is based on Reynold Averaged Navier-Stokes (RANS) equations in which the continuity and momentum equations are based on the time-averaged steady-state velocity of the fluid. It is easy to provide initial and/or boundary conditions in this model. However, it does not predict exactly where high eddies are developed. Nevertheless, the flow pattern and pressure distribution are mapped to a level of acceptable accuracy by introducing additional variables in the form of two transport equations. The one is the production of Turbulence Kinetic Energy (k) due to wind shear and buoyancy, and the second is Dissipation of Turbulence Kinetic Energy (ε) due to viscous forces. In the ANSYS (CFX) solver theory guide 2012.1, the equations of continuity and momentum of flow, and the two transport equations of the turbulence model $(k-\varepsilon)$, are explained in the manual [29].

4. Mean Velocity Characteristics

In nature, as explained earlier in Para 1, that an exponential velocity field along height within the ABL zone exists, it is difficult to define velocity load along building height.

However, certain equations have been developed for the gradient velocity field in ABL. The power law equation, as described below, is widely used in wind engineering experiments for representing ABL flow.

Power Law:

$$u = u_{Ref}\left(\frac{Z}{Z_{Ref}}\right)^{\alpha} \quad (2)$$

where, u_{Ref} = reference wind speed at 10 m/s. Z_{Ref} = reference height taken as 10 m. u = time-averaged longitudinal velocity at height Z above ground, and α is the terrain roughness coefficient. Though this equation is analytically not correct for the bottom 10 m of ABL, it provides a velocity of wind at higher altitudes well.

5. Computational Domain and Flow Parameter

The wind flow occurring in nature can be represented with good resemblance for the simulation when the computational domain is developed as recommended [30]. The computational domain was constructed as a parallelopiped large enough in all three directions, with the model placed inside the domain as shown in Figure 4a. Precaution was taken to keep the size of the domain large enough so that fluid reflections from the domain walls did not occur and abnormal wind pressure around the model did not happen. Simultaneously, it was ensured the blockage ratio did not increase above 3%. At the same time, domain size was not kept too large to restrict grid elements within reasonable numbers. More grid elements require greater computer facilities and more time for convergence of the numerical solution. A model of a diamond C-shape building with a plan area of 300 sqm and height of 50 m was created with a length scale of 1:100.

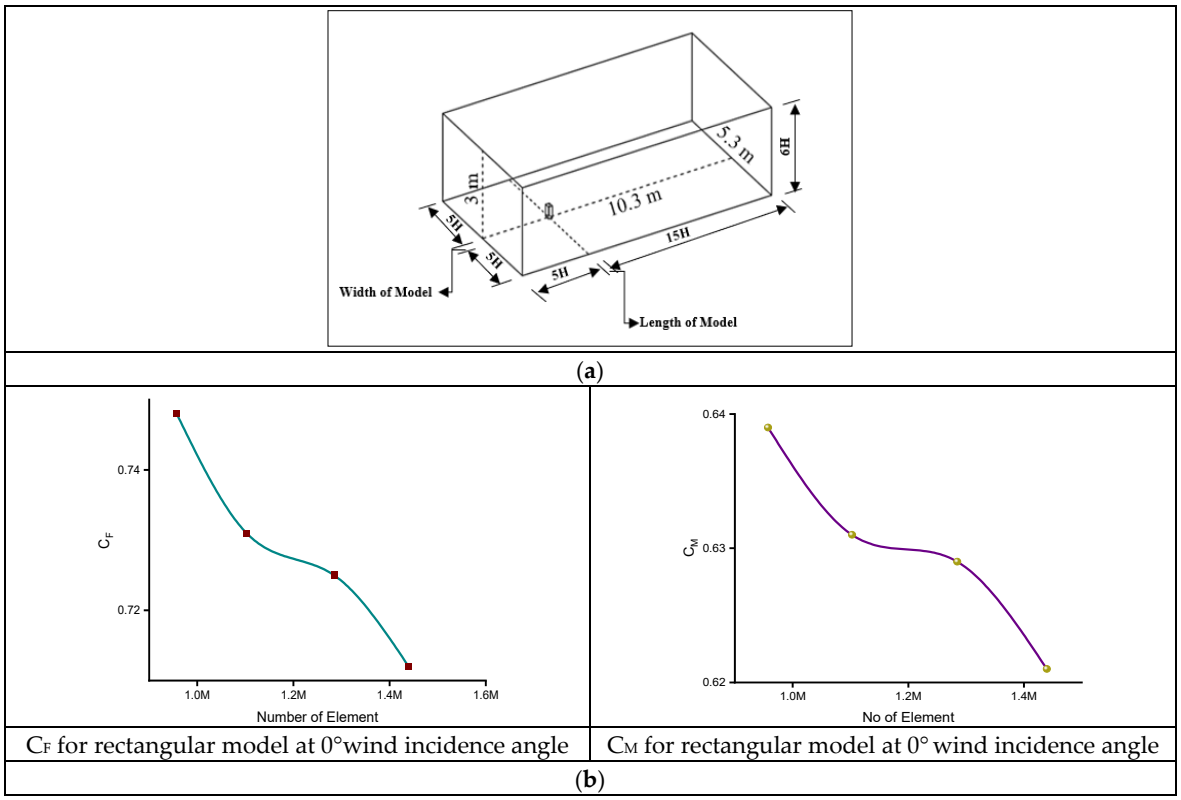

Figure 4. (**a**): Computational Domain, (**b**) Grid Sensitivity test graph.

6. Computational Grid and Grid Sensitivity

The mesh element size in the domain volume and surface of the model affected the convergence of the solution considerably. The grid resolution was set to precisely capture

crucial physical factors of the flow such as pressure on the surface of the model, separation of flow, formation of wake and vortices, reattachment of flow, and so on. The primary goal was to measure pressure on the surface of the model; hence, it was discretized into finer elements than the computational domain. The meshing technique for a better solution depended upon the approach to discretize the domain and model surface into smaller elements. In the present study, different regions of the domain were discretized with different element sizes and it was ensured the solution reached a steady-state [29]. The ratio of element size in the base was varied between 0.50 to 0.40 times the element size of the domain, and model face sizing was varied between 0.25 to 0.2 times the element size of the domain. However, with smaller mesh elements, solution took more time. A trade-off among them was adopted. The mesh elements on the model surface were inflated to achieve a smooth transition from the domain elements so that the velocity gradients could be mapped correctly near no-slip walls (Figure 5). Final results were adopted with 0.44 times the element size of the domain on the base and 0.22 times on model faces. At this resolution, the solution reached a steady-state, and the residual RMS error for mass and momentum convergence was achieved between 10^{-4} to 10^{-5} for momentum in the three directions and up to 10^{-6} for mass respectively. The corresponding domain imbalances in the values were 0.001% for momentum in the three directions and 0% for mass.

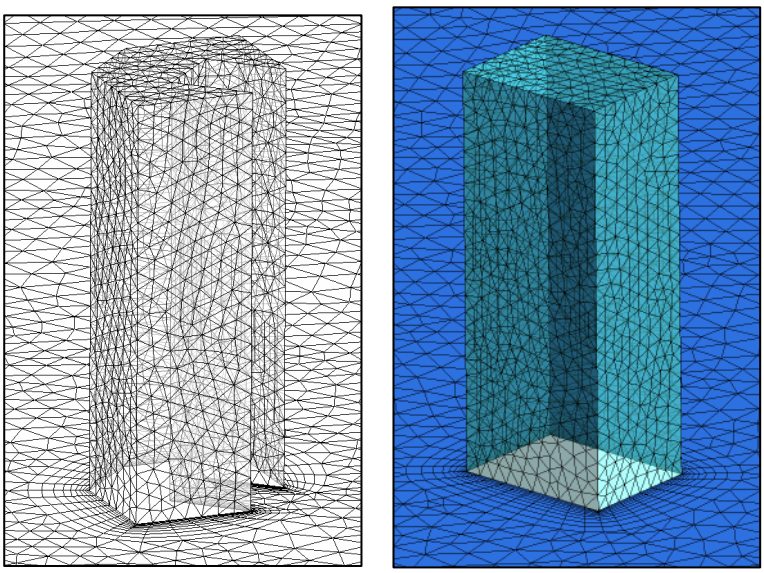

(**a**) (**b**)

Figure 5. Meshing Detail. (**a**) Diamond C-Shape Model. (**b**) Rectangular Model.

Validation is a crucial step in the examination of wind effects on tall buildings using ANSYS CFX. Its primary objective is to verify the accuracy and reliability of the results derived from numerical simulations; hence, in this study, the result for the grid sensitivity test is depicted in Figure 4b [31]. During this procedure, an independent reference model is constructed and assessed to compare and confirm the outcomes of the current study against the Indian Standard IS: 875 (part-3): 2015. This validation process ensures the precision and dependability of the simulation methodology employed in the present research, thereby enhancing the credibility of the results for the specific tall building in question. Additionally, it establishes a benchmark for future investigations, further strengthening the legitimacy of the simulation approach utilized in this study, which focuses on analysing wind effects on tall buildings with varying cross-sectional shapes.

7. Flow Parameters and Boundary Conditions

Homogeneous steady-state wind flow under ABL at the inlet of the domain was provided with α = 0.143. Free stream velocity at the roof of the model attained was found

to be 0.63 m/s. This velocity is sufficient to achieve critical R_e for turbulent flow around sharp-edged models like the present one. Figure 2 shows the velocity profile at the inlet, the wind profile in compared in the numerical simulation and the experimental wind profile obtained [20]. Free slip wall condition was provided on the domain side walls and top wall. The top of the model was also provided with a free slip wall condition. By providing this condition, it was ensured that flow parallel to the walls is free from frictional forces and is computable during the simulation. A no slip wall condition was provided on the model surfaces and the ground of the domain to ensure the velocity at the surface is zero for the making of boundary layer flow from the wall surfaces. To change the direction of the wind in a clockwise direction, the model is rotated in an anticlockwise direction with the same flow parameters and boundary conditions.

8. Result and Discussion

8.1. Flow Pattern

For unconventional building plan shapes, it is not guaranteed the critical coefficient of pressure on faces shall be in the orthogonal direction of wind flow. Variation in pressure on the surfaces of any obstacle encountered by the wind is influenced by wind flow patterns. Other mechanisms associated with the wind flow pattern, such as vortex generation, drag and uplift forces, local eddies and turbulences, and the formation of a shear layer on surfaces, interference effects, etc., also influence the coefficient of pressure. In the present paper, the values of surface pressures generated on the recessed faces D1, D2, and E of the model were evaluated to calculate the external mean coefficient of pressure (C_{Pe}) at wind incident angles 0°, 30°, 60°, 105°, 135°, and 180°. On these wind angles, critical values were plotted in the graph of area average C_{Pe} values on recessed faces (Figure 6). It is seen that the critical average suction pressure coefficient on the recessed faces D1, D2, and E are encountered at different angles of attack (AoA). The value of negative pressure on the faces is almost similar at 30° AoA. From 30° to 60°, they go on increasing marginally. From the AoA 60° onwards, the values are increasing substantially up to 105° AoA. However, the rate of increase of C_{Pe} on face D2 is more prominent than that on face D1. From there, the value of negative pressure on faces improves constantly and comes to nil between 120° and 135° AoA. From there, they change the sign and increase up to the AoA of 180°.

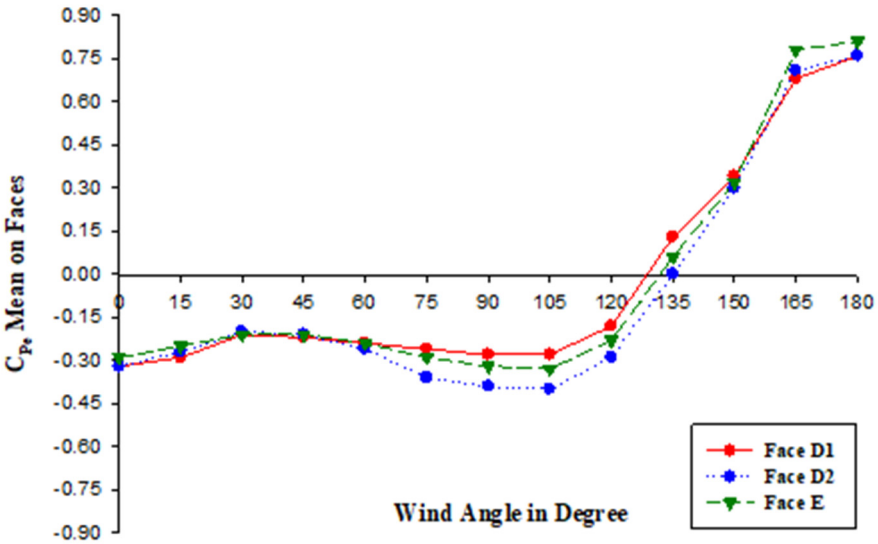

Figure 6. Variation of Mean C_{Pe} Values on Recessed Faces.

Figure 7a–f shows the pattern of wind flow for wind incident angles 0°, 30°, 60°, 105°, 135°, and 180°. Within the recessed well for the obliqued angle of flow, it is found that the flow is separated from the frontal corner and a shear layer is formed. The separated shear layer is rolling up and is evolving vortices. Instability associated with the laminar-turbulent

transition to turbulent flow on the suction side is seen creating vortices. The separated vortices are continuously hitting on the recessed surfaces. Creation of different wake and vortex on the leeward side, vortex and eddies within the opening/well of the recessed portion, separation of flow pattern from the side faces and edges, and the impact of wind on the windward side is different for different wind angles.

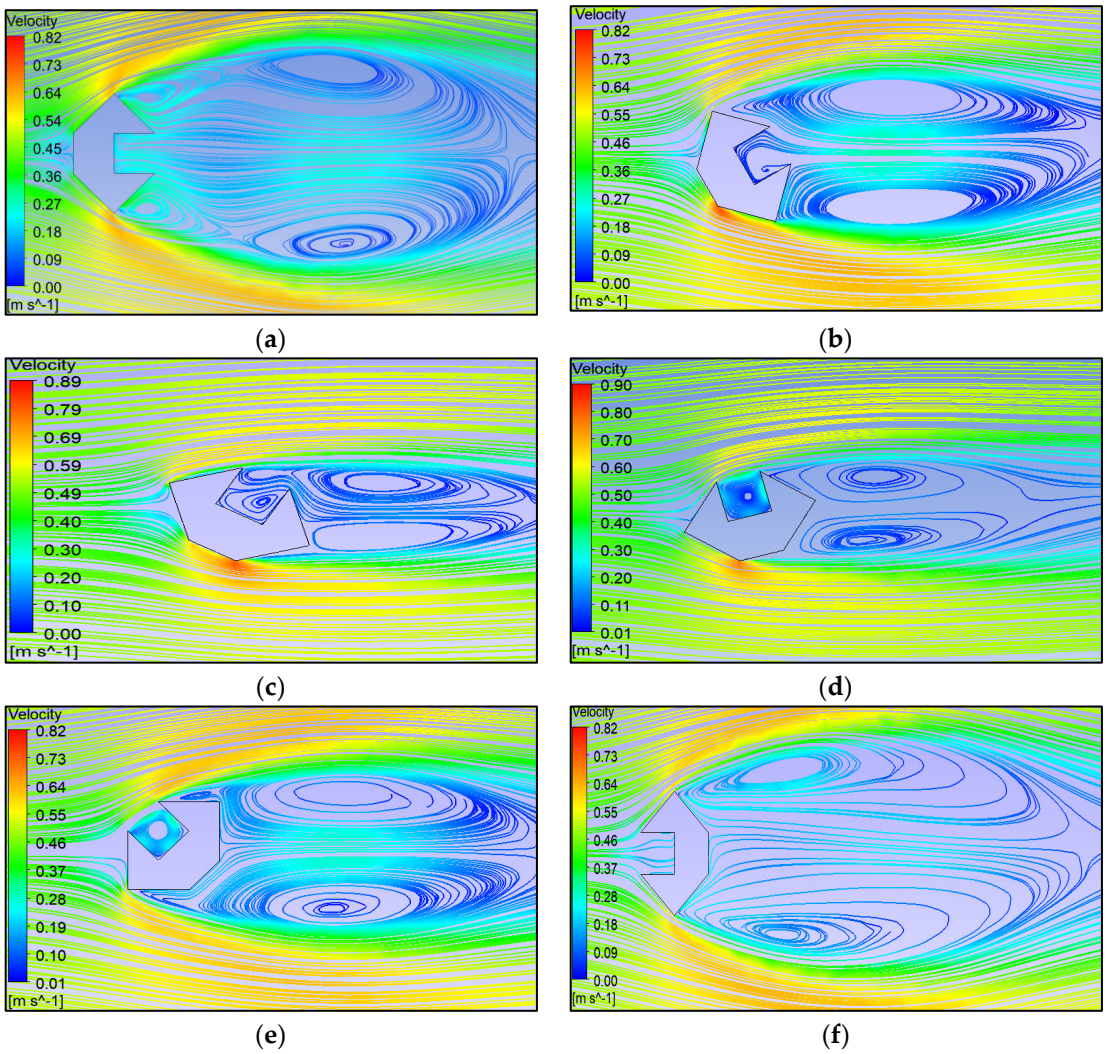

Figure 7. Wind Flow Pattern-Plan. (**a**) 0° AoA. (**b**) 30° AoA. (**c**) 60° AoA. (**d**) 105° AoA. (**e**) 135° AoA. (**f**) 180° AoA.

Figure 8a–f provides a comprehensive visualization of the wind patterns along the wind direction on a vertical plane, meticulously passing through the global origin of the model. These graphics vividly illustrate the intricate interplay of wind flow across the unique structural features of the model. A notable observation is the variability in the upwind ground vortex, which showcases distinct characteristics for different incident wind angles. Additionally, a discernible trend emerges as the variations in peak wind velocities across certain incident wind angles. This underscores the distinct response of the diamond C-shaped model in comparison to a conventional model with the same height and plan area. In particular, the coefficient of pressure distribution on the surfaces of our diamond C-shaped model is expected to exhibit marked differences. This expectation is attributed to the complex interferences among the faces of the recessed portion, denoted as face D1, D2, and E. The intricate geometry of the building model gives rise to unique aerodynamic effects, especially in these recessed areas, which are anticipated to significantly influence the pressure coefficients.

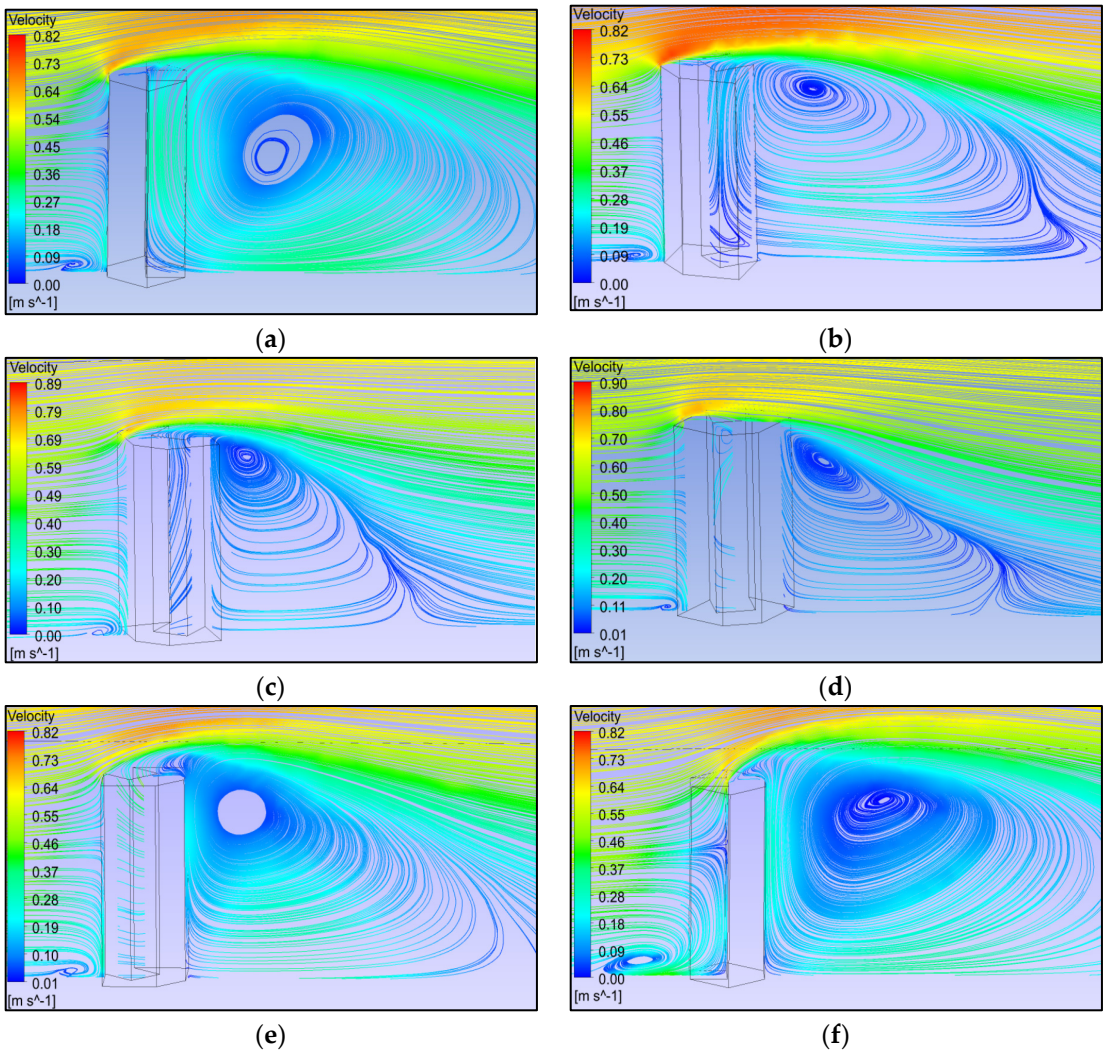

Figure 8. Wind Flow Pattern -Elevation on a Central Vertical Plane. (**a**) 0° AoA. (**b**) 30° AoA. (**c**) 60° AoA. (**d**) 105° AoA. (**e**) 135° AoA. (**f**) 180° AoA.

The results presented in Figure 8a–f offer valuable insights into the intricate wind behaviour surrounding the diamond C-shaped model. These findings emphasize the need for a comprehensive assessment of wind effects on non-standard building shapes, as this model response differs significantly from conventional structures. The complex wind effects among the recessed faces of the model, as evident on face D1, D2, and E, point to the importance of considering intricate geometries in wind engineering studies. This ultimately reaffirms the importance of tailored design and engineering solutions for non-standard structures, especially in areas where wind resilience is a crucial factor. It underscores the need for specialized attention to aerodynamic considerations in the design and construction of buildings with unconventional shapes.

8.2. Pressure Coefficient on Faces

The C_{Pe} contours on recessed faces for 0°, 30°, 60°, 105°, 135°, and 180° are presented in Figure 9a–f. Dissipation of wind energy by the incident wind on the windward face is found to cause positive pressure on the faces, whereas suction pressure on faces occurs due to vortex generation and uplift force created by backwash and/or sidewash. Figure 9f shows face E, which is the windward face for a 180° AoA, is subjected to the highest positive pressure. The C_{Pe} value is almost constant throughout the width of the faces up to the height of almost the rooftop of the model. The mean C_{Pe} value on the face is 0.78. Since the wind is entrapped and no flow separation from edges of face E is taking place,

except the rooftop, the C_{Pe} is almost constant on the face except nearer to the rooftop. The wind after impact on face E is reflecting and indulges with limb faces D1 and D2 creating an interference effect on them. After a height of 0.4 m C_{Pe} is reducing rapidly, Figure 10f, and becomes negative before it touches the rooftop where the separation of flow and the uplift force increases velocity. The recessed limb faces parallel to the wind flow, D1 and D2, are also experiencing positive pressure of constant nature throughout their widths as the wind is entrapped after hitting face E, and reflecting on faces D1 and D2. The mean C_{Pe} on the faces D1 and D2 are 0.74/0.75. For 0° AoA, Figure 11a, the value of mean suction pressures on all three faces increases up to a height between 0.3 and then again progressively decreases towards the rooftop. Concentration points of pressure are also seen on some faces. This is due to the fact that the two-dimensional structure of the shear layer changes into the three-dimensional structure by vortex instability.

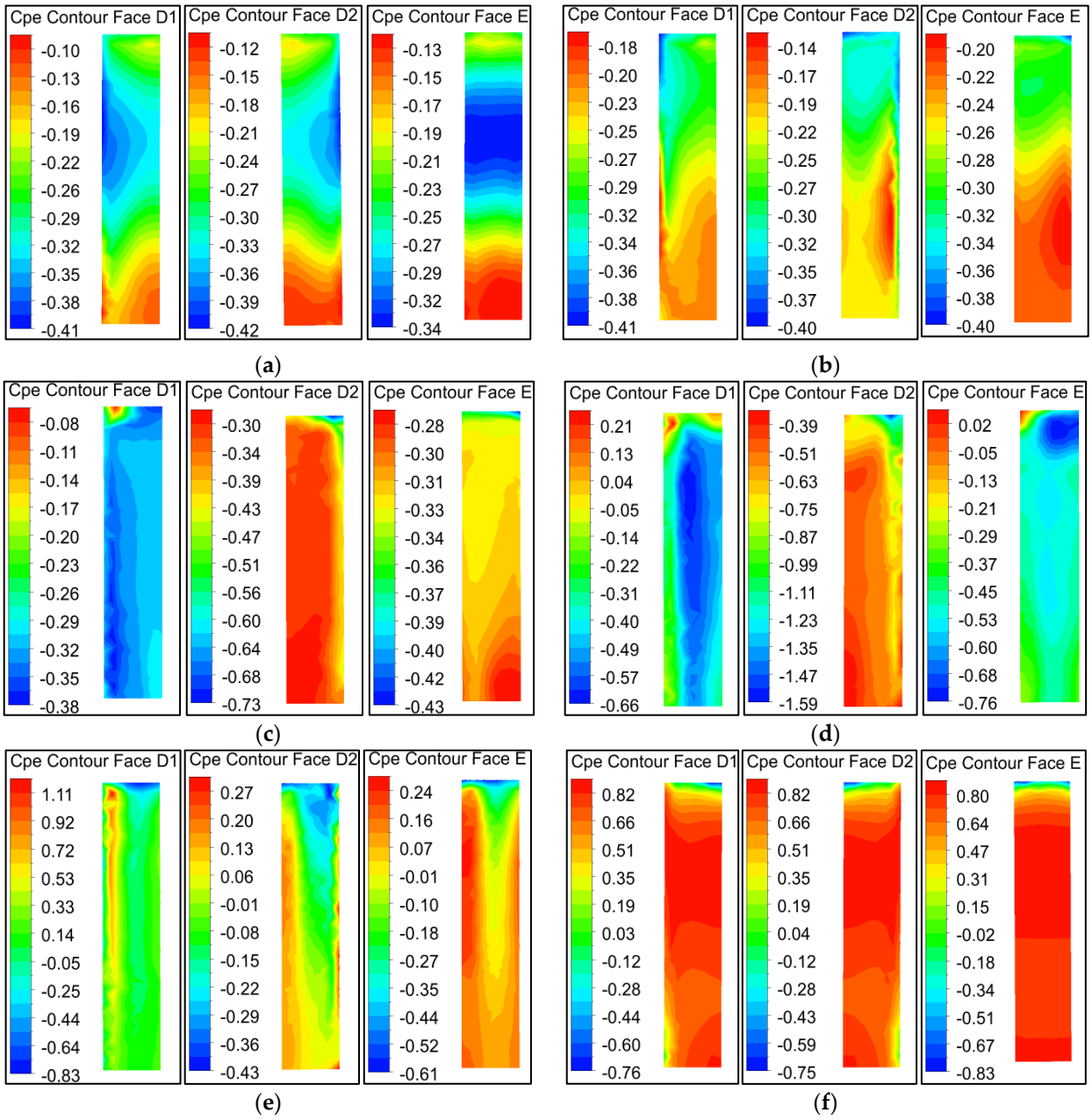

Figure 9. C_{Pe} Contour for C-shape building model. (**a**) C_{Pe} Contour 0° AoA. (**b**) C_{Pe} Contour 30° AoA. (**c**) C_{Pe} Contour 60° AoA. (**d**) C_{Pe} Contour 105° AoA. (**e**) C_{Pe} Contour 135° AoA. (**f**) C_{Pe} Contour 180° AoA.

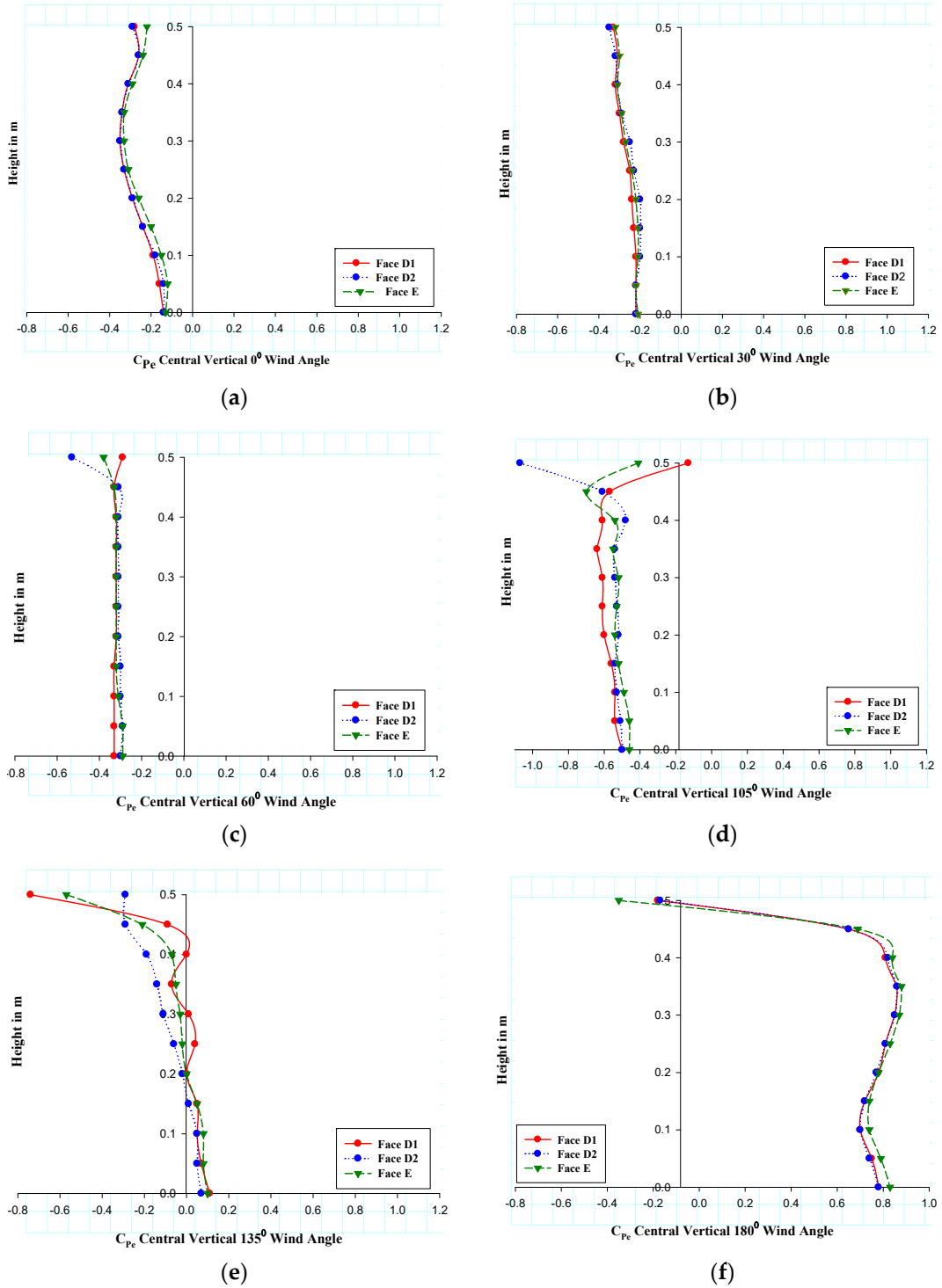

Figure 10. Variation of Pressure on Central Vertical Line for C-Shape building model. (**a**) Central Vertical C_{Pe} 0° AoA. (**b**) Central Vertical C_{Pe} 30° AoA. (**c**) Central Vertical C_{Pe} 60° AoA. (**d**) Central Vertical C_{Pe} 105° AoA. (**e**) Central Vertical C_{Pe} 135° AoA. (**f**) Central Vertical C_{Pe} 180° AoA.

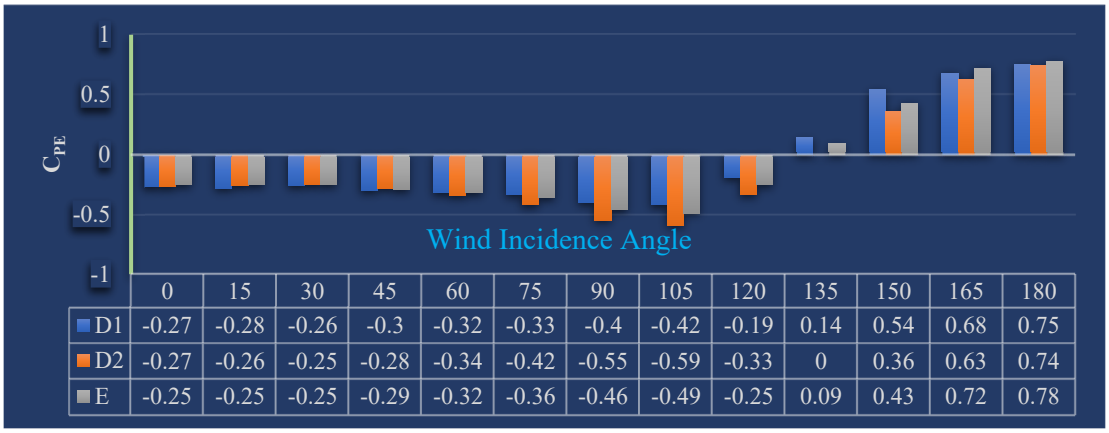

	0	15	30	45	60	75	90	105	120	135	150	165	180
D1	-0.27	-0.28	-0.26	-0.3	-0.32	-0.33	-0.4	-0.42	-0.19	0.14	0.54	0.68	0.75
D2	-0.27	-0.26	-0.25	-0.28	-0.34	-0.42	-0.55	-0.59	-0.33	0	0.36	0.63	0.74
E	-0.25	-0.25	-0.25	-0.29	-0.32	-0.36	-0.46	-0.49	-0.25	0.09	0.43	0.72	0.78

Figure 11. Comparative Study of C_{Pe} on Faces for Different AoA.

8.3. Pressure along Central Vertical Line

Such plots provide us with a realistic and fine picture of the pattern of pressure coefficients along the height of the faces, and changes in flow pattern along the height can also be understood from them. The central vertical pressure on faces is shown in Figure 10a–f. Positive pressure along the central vertical line on the model surfaces is positive where the faces are obstructing the flow. At 0° wind angle, the recessed faces facing suction follow the same path along the vertical line and overlap with one another. The suction increases up to the height of 0.3 m and then decreases due to greater uplift force. As the wind incident angle changes, the central vertical C_{Pe} value on all the three faces are becoming straighter, i.e., the C_{Pe} values are uniform. At a 60° wind angle, they are almost straight. Up to 105° wind angles, C_{Pe} values are negative. At 135° wind angle, the values are positive up to the height of 0.2 m and then grow to negative due to the channelizing effect along the height of the recessed well cavity. On face D1, fluctuations in the central vertical C_{Pe} is seen due to instability of microlevel turbulence and eddies created on the face. The C_{Pe} values on the faces are positive for 180° AoA and overlap with one another.

8.4. Comparative Study of C_{Pe} Values

A comparative study of average C_{Pe} values on the recessed faces D1, D2, and E is shown in Figure 11. It is seen that for 0° and 180° AoA, the coefficient of pressure on faces D1 and D2 is almost symmetrical as the flow pattern within the recessed well is symmetrical. The mean coefficient of pressure on the faces is also shown. The values change sign at 135° AoA with the minimum numerical values on all three faces: D1 (0.14), D2 (0.00), and E (0.09). At 60° AoA, all the three faces have almost equal average C_{Pe} values: D1 (−0.32), D2 (−0.34), and E (−0.32).

The maximum suction occurs at 105° AoA on faces. It is −0.42 on face D1, −0.59 on face D2 and −0.49 on face E. Therefore, a detailed investigation at different wind angles for unconventional plan shape buildings is a must on a case-to-case basis so the correct values may be incorporated during the design of cladding/glazing units.

9. Conclusions

The wind pressure data reported here is useful for identifying wind pressure distribution on the recessed sides of a C-plan diamond-shaped building. The present study has shown prominent output related to pressure (C_{Pe}) distributions on the recessed faces can be induced due to changes in wind incidence angle. Suction pressure in the recessed side for different wind incidence angles is discussed, and it is observed to be almost constant for less than 60° wind angle as flow tends to skip past the recess gap, leaving stagnant flow in the recessed cavity. The recessed faces are subjected to a uniform pressure field at a 60° wind incidence angle. Due to changes in the angle of wind incidence, the increased pressure

field turns out to be positive, and the minimum positive value of the mean coefficient of pressure on the faces is found to be at 135° wind incidence angle.

Wind flow patterns from ANSYS (CFX) based on the standard $k - \varepsilon$ turbulent model provide us with a good idea of the modification of wind flow around the bluff body. However, the quality of numerical results can be improved by making different meshing grid arrangements in various regions of flow as per expected turbulent characteristics in the region. Nevertheless, the results obtained can provide useful information about wind pressure distributions on such irregular plan shapes.

Author Contributions: Conceptualization, A.K. and R.K.M.; methodology, A.K., R.K.M. and R.R.; software, A.K., R.K.M. and R.R.; validation, R.R., M.I.K. and J.M.K.; formal analysis, A.K. and R.K.M.; Resources, M.I.K. and J.M.K.; writing—original draft, A.K.; writing—review and editing, R.R., R.K.M., M.I.K. and J.M.K.; supervision, R.R. All authors have read and agreed to the published version of the manuscript.

Funding: The authors extend their appreciation to Researcher Supporting Project number (RSPD2023R692), King Saud University, Riyadh, Kingdom of Saudi Arabia.

Data Availability Statement: Data are contained within the article.

Acknowledgments: The authors extend their appreciation to Researcher Supporting Project number (RSPD2023R692), King Saud University, Riyadh, Kingdom of Saudi Arabia.

Conflicts of Interest: The authors declare no conflict of interest.

References

1. Pradeep, R.K.; Ehsan, V.; Azadeh, S. *Computation Fluid Dynamics Approach for Highrise Buildings*; Report No. IIIT/TR/2013/-1; Centre for Earthquake Engineering, IIIT Hyderabad: Hyderabad, India, 2013; pp. 1–9.
2. Dryden, H.L.; Hill, G.C. Wind Pressure on Structures. In *Scientific Papers of the Bureau of Standards*; NIST: Gaithersbur, MD, USA, 1925; pp. 698–732.
3. Holmes, J.D. *Wind Loading of Structures*, 3rd ed.; CRC Press: Boca Raton, FL, USA, 2015.
4. Taranath, B.S. *Wind and Earthquake Resistant Buildings*; Marcel Dekker: New York, NY, USA, 2004.
5. Baines, W.D. *Effect of Velocity Distribution on Wind Loads on a Tall Building*; AIVC: Surrey, BC, Canada, 1952.
6. Gomes, M.G.; Rodrigues, A.M.; Mendes, P. Experimental and numerical study of wind pressures on irregular-plan shapes. *J. Wind. Eng. Ind. Aerodyn.* **2005**, *93*, 741–756. [CrossRef]
7. Cheng, C.C.K.; Lam, K.M.; Leung, A.; Cheng, C.C.; Lam, K.; Leung, A.Y. Wind Flow in the Recessed Cavities of a Tall Building. 2009. Available online: https://www.researchgate.net/publication/255566643 (accessed on 5 October 2023).
8. Xu, Z.; Yin, J. The Influence of Aeroelastic Effects on Wind Load and Wind-Induced Response of a Super-Tall Building: An Experimental Study. *Buildings* **2023**, *13*, 1871. [CrossRef]
9. Amin, J.A.; Ahuja, A.K. Experimental Study of Wind-Induced Pressures on Buildings of Various Geometries. 2011. Available online: www.ijest-ng.com (accessed on 5 October 2023).
10. Amin, J.A.; Ahuja, A.K. Mean interference effects between two buildings: Effects of close proximity. *Struct. Des. Tall Spec. Build.* **2011**, *20*, 832–852. [CrossRef]
11. Tanaka, H.; Tamura, Y.; Ohtake, K.; Nakai, M.; Kim, Y.C.; Bandi, E.K. Experimental Investigation of Aerodynamic Forces and Wind Pressure Acting on Tall Buildings with Various Unconventional Configuration. *J. Wind. Eng. Ind. Aerodyn.* **2013**, *107–108*, 179–191. [CrossRef]
12. Zhao, S.; Zhang, C.; Dai, X.; Yan, Z. Review of Wind-Induced Effects Estimation through Nonlinear Analysis of Tall Buildings, High-Rise Structures, Flexible Bridges and Transmission Lines. *Buildings* **2023**, *13*, 2033. [CrossRef]
13. Kheyari, P.; Dalui, S.K. Estimation of Wind Load on a Tall Building under Interference Effect. *Jordon J. Civ. Eng.* **2014**, *9*, 84–101.
14. Meena, R.K.; Raj, R.; Anbukumar, S. Effect of wind load on irregular shape tall buildings having different corner configuration. *Sadhana Acad. Proc. Eng. Sci.* **2022**, *47*, 126. [CrossRef]
15. Kar, R.; Dalui, S.K. Wind interference effect on an octagonal plan shaped tall building due to square plan shaped tall buildings. *Int. J. Adv. Struct. Eng.* **2016**, *8*, 73–86. [CrossRef]
16. Charisi, S.; Thiis, T.K.; Aurlien, T. Full-scale measurements of wind-pressure coefficients in twin medium-rise buildings. *Buildings* **2019**, *9*, 63. [CrossRef]
17. Yan, B.; Li, Y.; Li, X.; Zhou, X.; Wei, M.; Yang, Q.; Zhou, X. Wind Tunnel Investigation of Twisted Wind Effect on a Typical super-tall building. *Buildings* **2022**, *12*, 2260. [CrossRef]
18. Bairagi, A.K.; Dalui, K. Comparison of Pressure Coefficient between Square and Setback Tall Building Due to Wind Load. In Proceedings of the 11th Structural Engineering Convention, Kolkata, India, 19–21 December 2018; pp. 1–6. Available online: https://www.researchgate.net/publication/329786479 (accessed on 5 October 2023).

19. Bhattacharyya, B.; Dalui, S.K. Investigation of mean wind pressures on 'E' plan shaped tall building. *Wind. Struct. Int. J.* **2018**, *26*, 99–114. [CrossRef]
20. Nagar, S.K.; Raj, R.; Dev, N. Experimental study of wind-induced pressures on tall buildings of different shapes. *Wind. Struct.* **2020**, *31*, 441–453.
21. Pan, H.; Wu, J.; Fu, J. Monitoring of Wind Effects on a Super-Tall Building under a Typhoon. *Buildings* **2023**, *13*, 47. [CrossRef]
22. Mallick, M.; Mohanta, A.; Kumar, A.; Raj, V. Modelling of Wind Pressure Coefficients on C-Shaped Building Models. *Model. Simul. Eng.* **2018**, *2018*, 6524945. [CrossRef]
23. Amin, J.A.; Ahuja, A.K. Characteristics of wind forces and responses of rectangular tall buildings. *Int. J. Adv. Struct. Eng.* **2014**, *6*, 66. [CrossRef]
24. *IS: 875: Part-3:2015*; Design Loads (Other than Earthquake) for Buildings and Structures—Code of Practice Part 3 Wind Loads (Third Revision). BIS: New Delhi, India, 2015.
25. *ASCE/SEI 7−22*; Minimum Design Loads and Associated Criteria for Building and Other Structure. 20191-4400. American Society of Civil Engineers: Reston, Virginia, 2017.
26. *AS/NZS-1170.2 (2002)*; Structural Design Actions, Part-2: Wind Actions. Standards Australia: Sydney, NSW, Australia; Standards New Zealand: Wellington, New Zealand, 2002.
27. *EN: 1991-1-4*; Eurocode-1: Actions on Structures-Part 1-4: General Actions-Wind Actions. Management Centre: Brussels, Belgium, 2010.
28. *BS: 6399-2*; Loading for Buildings. Code of Practice for Wind Loads (Incorporating Amendment No. 1 and Corrigendum No. 1). British Standards Institution: London, UK, 1997.
29. ANSYS Inc. *ANSYS CFX-Solver Theory Guide*; ANSYS Inc.: Canonsburg, PA, USA, 2009. Available online: http://www.ansys.com (accessed on 5 October 2023).
30. Revuz, J.; Hargeaves, D.M.; Owen, J.S. On the Domain Size for the Steady State CFD Modeling of a Tall Building. *Wind. Struct.* **2012**, *15*, 313–329. [CrossRef]
31. Paswan, A.P.; Jayant, B.; Rukhaiyar, A.; Dahiya, K.; Raj, R.; Meena, R.K. Estimations of Wind-Generated Effects on a Regular Tower of Varying Cross-Sectional Shape. *J. Inst. Eng. Ser. A* **2023**. [CrossRef]

Disclaimer/Publisher's Note: The statements, opinions and data contained in all publications are solely those of the individual author(s) and contributor(s) and not of MDPI and/or the editor(s). MDPI and/or the editor(s) disclaim responsibility for any injury to people or property resulting from any ideas, methods, instructions or products referred to in the content.